A Modulation Method With Current Zero-Crossing Distortion Elimination and Voltage Balance Control for the RSHMC Converter

Guangtao Zhou, *Student Member, IEEE*, Xiangyang Xing, *Member, IEEE*, Hao Liu, *Student Member, IEEE*, Shuai Zhang, *Member, IEEE*, Xiangjun Li, *Senior Member, IEEE*, and Rui Zhang, *Student Member, IEEE*

***Abstract*—Hybrid multilevel converters have gained more popularity due to their unique superiority. Thus, the reduced switch hybrid multilevel (RSHMC) converter is adopted in this article which consists three H-bridge cells and a Vienna rectifier. The RSHMC converter combines the advantages of these two topologies and can output higher voltage level by adopting fewer switching devices compared with other multilevel converters. However, the Vienna rectifier of the RSHMC converter has the inherent current zero-crossing distortion (CZCD) problem, which will increase the total harmonic distortion of the grid-side current. Thus, a modulation method based on phase disposition-pulsewidth modulation is proposed to eliminate the CZCD of the RSHMC converter by selecting redundant switching states. Besides, in order to ensure the normal operation of the RSHMC converter, the proposed modulation method can also realize the voltage balance control of the floating capacitor and the neutral point which is also realized by selecting the switching states to charge or discharge. Consequently, the RSHMC converter can operate normally with balanced voltage and without CZCD after adopting the proposed modulation method. Finally, the feasibility and correctness of the proposed modulation method are verified by simulation and experimental results.**

***Index Terms*—Current zero-crossing distortion (CZCD) elimination, hybrid multilevel converter, voltage balance control of floating capacitors and neutral point.**

I. Introduction

MULTILEVEL converters including the neutral point clamped converter [1], [2], the cascaded H-bridge (HB) converter [3], [4], [5], [6], and the floating capacitor converters [7], [8], have gained widespread application in practical settings for their distinct advantages over two-level converters. These advantages mainly include: lower voltage stress, higher efficiency, as well as higher output voltage, and so on [9], [10]. However, each topology has its own specific advantages and drawbacks. Thus, the hybrid multilevel converters are utilized to enhance performance and mitigate shortcomings by combining the features of several different topologies [11].

In recent years, the Vienna rectifier has been widely applied due to its low cost, high power density, and high reliability feature [12]. Meanwhile, HB has the advantage of high scalability which can increase the number of output voltage levels without independent dc source [13]. Thus, the reduced switch hybrid multilevel (RSHMC) converter in [14] is adopted in this article which consists of a Vienna rectifier and three cascaded HBs.

Compared with other hybrid multilevel converters in [15], [16], [17], and [18], the RSHMC converter has advantages over them. For convenience, Table I compares maximum switching voltage stress, number of insulated gate bipolar transistors (IGBTs) and diodes, number of the floating capacitors, bidirectional capability, number of independent dc source and output voltage levels. Table I gives that the RSHMC converter has fewer active switching devices which stress less maximum voltage than other hybrid multilevel converters. When the output voltage level is identical, the RSHMC converter has less floating capacitors and no independent dc source which reduces the difficulty of control and decreases the cost. Details are given in Table I.

However, the RSHMC converter has the current zero-crossing distortion (CZCD) problem due to the phase difference between the voltage reference and the current, which will lead to erroneous voltage pulses near the current zero-crossing point and increase the total harmonic distortion (THD) of the grid-side current [19], [20]. Numerous approaches have been proposed for Vienna rectifier, which is also applicable to the RSHMC converter to eliminate or mitigate the CZCD. The approaches can be organized into two primary categories: control method and modulation method.

Among the control methods, the hysteresis switching methods are proposed for controlling the input currents as sinusoidal waveforms [21], [22], [23], [24]. In [21] and [24], the sinusoidal reference current and its hysteresis band are used to operate the switching device. However, the hysteresis switching methods do not guarantee a constant switching frequency in the input voltage. Besides, the reactive power compensation method can

Received 29 March 2024; revised 10 July 2024; accepted 16 August 2024. Date of publication 23 August 2024; date of current version 7 October 2024. This work was supported in part by the National Natural Science Foundation of China under Grant 62222309, in part by the Natural Science Foundation of Shandong under Grant ZR2022JQ29, and in part by the National Natural Science Foundation of China under Grant 62173210, Grant 61821004, Grant 62273207, and Grant 623B2069. Recommended for publication by Associate Editor G. Konstantinou. *(Corresponding author: Xiangyang Xing)*

Guangtao Zhou, Xiangyang Xing, Hao Liu, Shuai Zhang, and Rui Zhang are with the School of Control Science and Engineering, Shandong University, Jinan 250061, China (e-mail: 202214790@mail.sdu.edu.cn; xyxing@sdu.edu.cn; 202034933@mail.sdu.edu.cn; spritstronger@sdu.edu.cn; sduzr2021@mail.sdu.edu.cn).

Xiangjun Li is with China Electric Power Research Institute, Beijing 100192, China (e-mail: lixiangjun@epri.sgcc.com.cn).

Color versions of one or more figures in this article are available at https://doi.org/10.1109/TPEL.2024.3448352.

Digital Object Identifier 10.1109/TPEL.2024.3448352

TABLE I
COMPARISON OF DIFFERENT MULTILEVEL CONVERTERS

Topology	Maximum switching voltage stress	Number of IGBTs	Number of diodes	Number of the floating capacitors	Bidirectional capability	Number of independent DC source	Output Voltage levels
CHB in [15]	$U_{dc}/4$	36	0	9	Yes	9	7
HNPC in [16]	U_{dc}	24	6	3	Yes	0	5
T^{2}C-HB in [13]	U_{dc}	24	0	3	Yes	0	7
ANPC-H in [17]	U_{dc}	30	0	3	Yes	0	7
NNPC in [18]	U_{dc}	30	0	9	Yes	0	7
RSHMC converter	$U_{dc}/4$	18	6	3	No	0	7

guarantee the same phase of the current and the reference voltages, which also can completely solve CZCD problem. However, this method achieves less power factor [25]. Furthermore, there is high controller complexity and computational burden in most of the control methods. Thus, the modulation method gains more popularity in practical.

Among modulation methods, the carrier-based pulsewidth modulation (CBPWM) in [12] is widely used in three-level topologies, which is easy to implement. For the CBPWM, the reference voltages are modified to satisfy their control aims. However, there are large ripples and low dc voltage utilization rates. The discontinuous pulse width modulation (DPWM) in [26], [27], and [28] is a common modulation strategy for the Vienna rectifier which has less switching loss. It is realized by calculating clamping angles and injecting offset voltage. However, there are large harmonics in the output current and the neutral current appears large fluctuations under DPWM. The space vector pulsewidth modulation (SVPWM) in [29] and [30] not only improves the voltage utilization rate but has advantages in control flexibility. The control aims can be realized by rationally selecting different switching state vector. However, it is difficult to implement in real systems because the SVPWM method has heavy calculation burden. Thus, a modulation method based on selecting different switching states is proposed in this article to solve the CZCD problem of the RSHMC converter which is not only easy to implement but has a better performance compared with most of the modulation method.

Furthermore, the voltage balance of the floating capacitors and the neutral point are the key factors to influence the normal operation of the RSHMC converter. And the voltage balance part of the proposed modulation method to control the floating capacitors and the dc-link are coupling which are also realized by selecting the switching states to charge or discharge the capacitors. Thus, since the balance of the floating capacitor voltage is controlled independently by each phase, it has higher priority and greater importance than the neutral point voltage to control its balance [31]. To realize the voltage balance control of the floating capacitors and the neutral point, the proposed modulation method set a threshold to decouple them and set two corresponding signals to feedback. Consequently, the proposed modulation method can realize the voltage balance while eliminating the CZCD by reasonably selecting the switching states.

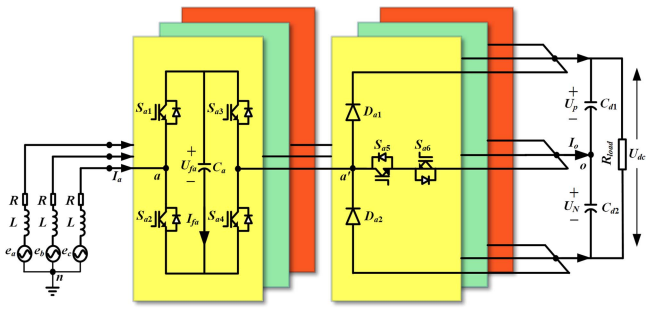

Fig. 1. Three phases of the RSHMC converter.

Therefore, in this article, a modulation method with CZCD elimination and voltage balance control for the RSHMC converter is proposed. The main innovations and contributions of this article are summarized as follows.

1) In the proposed modulation method, the CZCD in the output current of the RSHMC converter can be eliminated by reasonably selecting the switching states with less computation and control difficulty.
2) The proposed modulation method can control the voltage balance of the floating capacitor and the neutral point which is also realized by selecting the redundant switching states. Furthermore, the voltage balance of the floating capacitors and the neutral point and the elimination of the CZCD can be achieved at the same time, which can ensure the normal operation of the RSHMC converter.

The rest of this article is organized as follows. In Section II, the overview of the RSHMC converter is proposed. Sections III and IV propose modulation method to eliminate CZCD and control the voltage balance. In Section V, the effectiveness of the proposed method is verified by simulation and experimental results. Finally, Section VI concludes this article.

II. OVERVIEW OF THE RSHMC CONVERTER

A. Topology of the RSHMC Converter

Fig. 1 shows the RSHMC converter, consisting of an HB and a Vienna rectifier per phase. The ac-side is connected to the three-phase grid e_x ($x = a,b,c$), and the dc-side is connected to the load. L is the filter inductance and R is the equivalent resistance. C_x ($x = a,b,c$) is the floating capacitor of HB and C_{d1}, C_{d2} are

respectively the upper and lower capacitor of the dc-side. S_{x1}, S_{x2} ($x = a,b,c$) and S_{x3}, S_{x4} ($x = a,b,c$) are two pairs of IGBT switches that operate in a complementary state respectively. S_{x5} and S_{x6} ($x = a,b,c$) have the same switching state, and D_{x1} and D_{x2} ($x = a,b,c$) are diodes which are uncontrollable. The output voltage of the RSHMC converter U_{xo} ($x = a,b,c$) consists of two parts, the output voltage of the HB $U_{xx'}$ ($x = a,b,c$) and the output voltage of the Vienna rectifier $U_{x'o}$ ($x = a,b,c$), which can be expressed as

$$U_{xo} = U_{xx'} + U_{x'o}. \tag{1}$$

The voltage of floating capacitor is defined as U_{fx} ($x = a,b,c$) and the voltage of dc-side is defined as $U_{\rm dc}$. And the voltages of C_{d1} and C_{d2} are, respectively, defined as U_P and U_N. Besides, the input current is defined as I_x ($x = a,b,c$) and the current flowing into the floating capacitor C_x is defined as i_{fx} ($x = a,b,c$). Provided the voltage across C_{d1} and C_{d2} in Fig. 1 is $2E$ and the output voltage amplitude of HB part is set as E. In rated condition, U_{fx} is controlled at E and U_P and U_N are respectively controlled at $2E$. Thus, the voltage of dc-side can be expressed as

$$U_{\rm dc} = U_P + U_N = 2U_P = 4E. \tag{2}$$

B. Mathematical Model

In this section, according to the proposed topology shown in Fig. 1, the continuous-time mathematical model of the proposed converter output phase voltages, and i_{fx} is expressed as follows.

The switching functions of the proposed topology can be expressed as

$$S_{xj} = \begin{cases} 1 & S_{xj} \text{ is ON} \\ 0 & S_{xj} \text{ is OFF} \end{cases}, \ x = a,b,c, \text{ and } j = 1 \sim 6\ . \tag{3}$$

Combined with the switching functions, the output phase voltage of the HB $U_{xx'}$ can be expressed as

$$U_{xx'} = (S_{x1} - S_{x3}) \cdot \frac{U_{\rm dc}}{4}, x = a,b,c. \tag{4}$$

The output voltage of the Vienna rectifier $U_{x'o}$ can be expressed as

$$U_{x'o} = \text{sgn}(i_x) \cdot (1 - S_{x5} \cdot S_{x6}) \cdot \frac{U_{\rm dc}}{2}, x = a,b,c \tag{5}$$

where sgn(i_x) is the symbolic function which is expressed as

$$\text{sgn}(i_x) = \begin{cases} 1 & \text{if } i_x > 0 \\ -1 & \text{if } i_x \le 0 \end{cases}, \ x = a,b,c. \tag{6}$$

Thus, the output voltage of the RSHMC converter U_{xo} can be expressed as

$$U_{xo} = (S_{x1} - S_{x3}) \cdot \frac{U_{\rm dc}}{4} + \text{sgn}(i_x) \cdot (1 - S_{x5} \cdot S_{x6}) \cdot \frac{U_{\rm dc}}{2}. \tag{7}$$

As shown in Fig. 1, according to the Kirchhoff's law of voltage, the output phase voltage equations of the RSHMC converter can be expressed as

$$e_x = L\frac{di_x}{dt} + Ri_x + U_{xo} + U_{\rm on}, x = a,b,c \tag{8}$$

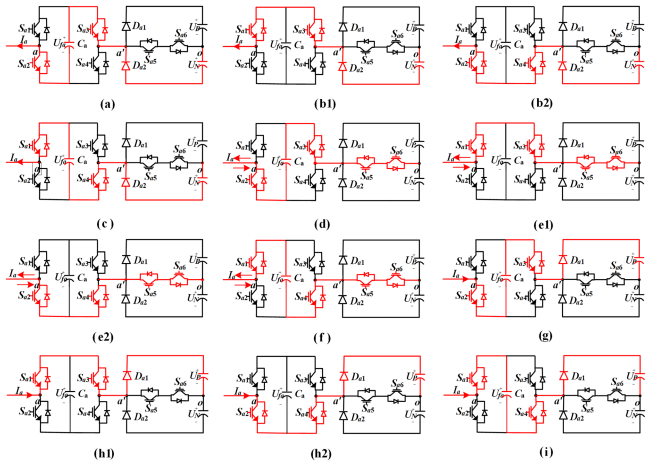

Fig. 2. Conduction paths of the RSHMC converter. (a) U_{ao} = -3E (I_a<0). (b1) U_{ao} = -2E (I_a<0). (b2) U_{ao} = -2E (I_a<0). (c) U_{ao} = -E (I_a<0). (d) U_{ao} = -E (I_a<0 or I_a>0). (e1) U_{ao} = 0 (I_a<0 or I_a>0). (e2) U_{ao} = 0 (I_a<0 or I_a>0). (f) $U_{ao} = E$ (I_a<0 or I_a>0). (g) $U_{ao} = E$ (I_a>0). (h1) U_{ao} = 2E (I_a>0). (h2) $U_{ao} = 2E$ (I_a>0). (i) $U_{ao} = 3E$ (I_a>0).

where $U_{\rm on}$ is the common mode voltage across the neutral-point of dc-side and three-phase input voltages.

According to the Kirchhoff's law of current, the input currents are expressed as

$$I_a + I_b + I_c = 0. \tag{9}$$

Based on the relationship between capacitor voltage and current, i_{fx} can be expressed as

$$i_{fx} = C_x \frac{dU_{fx}}{dt}, x = a,b,c. \tag{10}$$

C. Switching States

Fig. 2 shows the conduction paths of seven-level output voltage in phase A. The red path represents the current path and the arrow direction represents the available direction of I_a. After analysis, HB can output 0 level and $\pm E$ level and the Vienna rectifier can output 0 level and $\pm 2E$ level. After cascading these two parts, the RSHMC converter can output seven levels from -3E to +3E. The switching states of the RSHMC converter are given in Table II, where 1 means that the switching device is ON and 0 means OFF. Table II gives that there are two conduction paths except $\pm 3E$ voltage level. However, only the redundant switching states of $\pm E$ voltage level can be utilized to control voltage balance of C_{d1}, C_{d2}, and C_a which are essential to attain accurate and steady output voltage. In order to facilitate analysis, Table II highlights the output voltage levels that are relevant to the floating capacitor voltage in orange and those that are not in yellow. Besides, since the two states of st2, st5, and st8 have the same influence on the floating capacitor voltage and the neutral point voltage. For facilitating analysis, they are combined into one state in this article which are st2, st5, and st8.

TABLE II
SWITCH STATES OF THE RSHMC CONVERTER

Output Voltage	Switching State	H-bridge rectifier				Vienna rectifier	
		S_{x1}	S_{x2}	S_{x3}	S_{x4}	S_{x5}	S_{x6}
3*E*	st9	1	0	0	1	0	0
2*E*	st8	1	0	1	0	0	0
2*E*	st8	0	1	0	1	0	0
E	st7	0	1	1	0	0	0
E	st6	1	0	0	1	1	1
0	st5	1	0	1	0	1	1
0	st5	0	1	0	1	1	1
-*E*	st4	0	1	1	0	1	1
-*E*	st3	1	0	0	1	0	0
-2*E*	st2	1	0	1	0	0	0
-2*E*	st2	0	1	0	1	0	0
-3*E*	st1	0	1	1	0	0	0

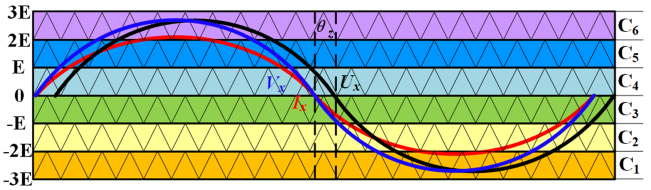

Fig. 3. Phase reference voltage and current over a fundamental period of PD-SPWM.

III. MODULATION METHOD WITHOUT CURRENT ZERO-CROSSING DISTORTION

A. Design of Modulation Method

In order to facilitate analysis and implementation, the RSHMC converter adopts the multilevel SPWM modulation method in this article, which is the most common method in multilevel converter modulation. In multilevel converters, carrier-based modulation methods can be divided into two classes: phase-shifted pulsewidth modulation (PS-PWM) and level-shifted pulsewidth modulation (LS-PWM). LS-PWM gains more popularity since it has better output voltage quality with lower distortion compared with PS-PWM.

There are three schemes for the LS-PWM: alternative phase opposite disposition; phase opposite disposition; and phase disposition (PD). When adopting PD-PWM modulation method, it has better performance in reducing distortion. Thus, the RSHMC converter adopts PD-PWM modulation method and the reference voltage and current in one phase over a fundamental period of PD-SPWM is shown in Fig. 3. The three-phase reference voltage (U_a, U_b, U_c) can be expressed as

$$\begin{cases} U_a = V_m \cos(2\pi f_s t) \\ U_b = V_m \cos(2\pi f_s t - 2\pi/3) \\ U_c = V_m \cos(2\pi f_s t + 2\pi/3) \end{cases} \tag{11}$$

where V_m is the magnitude of the source, and f_s is the fundamental frequency of the source.

PD-PWM modulation method requires six triangular carriers of the same amplitude and frequency which are, respectively, defined as C_1–C_6, as shown in Fig. 3. The relationship between voltage level, modulation wave and carrier wave are shown in Table III. Besides, the modulation index m of the modulation wave is defined as

$$m = \frac{\sqrt{3}V_g}{U_{\rm dc}} \tag{12}$$

where V_g is the peak value of the grid e_x.

TABLE III
RELATIONSHIP BETWEEN VOLTAGE LEVEL, MODULATION WAVE AND CARRIER WAVE

Relationship between modulation wave and carrier wave	Voltage level
$U_x \geqslant C_6$	3E
$C_5 \leqslant U_x < C_6$	2E
$C_4 \leqslant U_x < C_5$	E
$C_3 \leqslant U_x < C_4$	0
$C_2 \leqslant U_x < C_3$	-E
$C_1 \leqslant U_x < C_2$	-2E
$U_x < C_1$	-3E

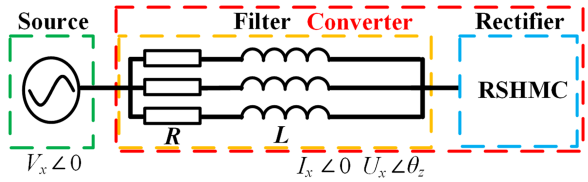

Fig. 4. Equivalent circuit of the RSHMC converter.

B. Analysis of Current Zero-Crossing Distortion

The current should be satisfied for normal operation of the RSHMC converter. However, when adopting the conventional PD-SPWM method, there will be current distortion in the RSHMC converter when the reference voltage U_x has phase difference with the current. Take the RSHMC converter operating with unity power factor as an instance, the phase of the current I_x will correspond with the phase of the source voltage V_x by applying control. Due to the existence of the filter inductor, the reference voltage U_x, which generates the pole voltage U_{xo} ($x = a,b,c$), has the phase difference with the current, as shown in Fig. 3. The phase difference between the current and reference voltage is defined as θ_z and with the increase of the inductor, θ_z will also be increased [32].

To calculate θ_z, the equivalent circuit between the RSHMC converter and the source is used, as shown in Fig. 4. This article only takes into account the filter inductance and resistance.

I_x of Fig. 4 can be expressed as

$$\frac{V_x - U_x}{Z} = \frac{V_x\angle 0 - U_x\angle\theta_z}{R + j2\pi f_s L} = I_x\angle 0 \tag{13}$$

where V_x is the output voltage of source, R is the resistance of the filter, and L is the inductance of the filter. Equation (13) can be expressed as

$$U_x\angle\theta_z = (V_x - RI_x) - j2\pi f_s L I_x. \tag{14}$$

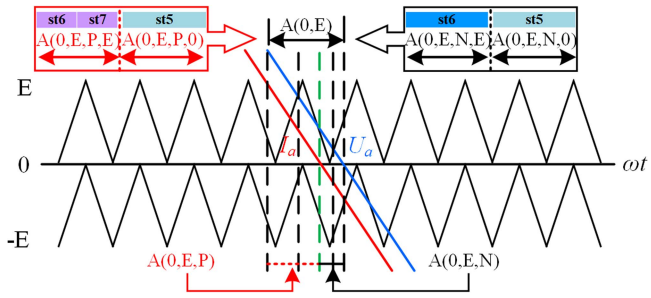

Fig. 5. Modulation wave across from positive to negative half cycle.

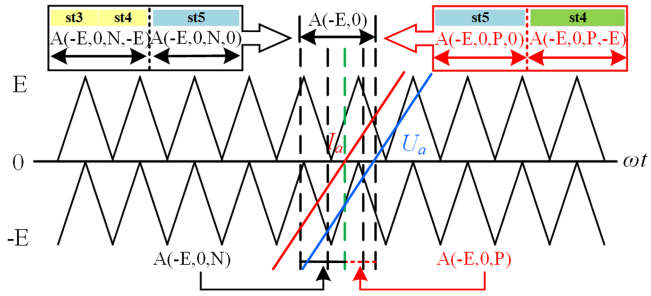

Fig. 6. Modulation wave across from negative to positive half cycle.

By using (13), θ_z is calculated as

$$\tan\theta_z = \frac{-I_x \times 2\pi f_s L}{V_x - I_x R} \tag{15}$$

$$\theta_z = \tan^{-1}\left(\frac{-I_x \times 2\pi f_s L}{V_x - I_x R}\right). \tag{16}$$

Since the phase of the current is θ_z ahead of the phase of the voltage, the current will cross the zero point in advance. Due to the existence of the Vienna rectifier in the RSHMC converter, when the polarity of I_x and U_x are inconsistent, the output voltage will deviate from the modulated wave resulting in the CZCD. In order to ensure the normal operation of the RSHMC converter, it is significant to eliminate the CZCD. For control techniques, the traditional reactive power compensation method can reduce θ_z or even can guarantee the same phase of the current and the reference voltages, which can completely solve the CZCD problem. However, the traditional reactive power compensation method achieves less power factor. For most modulation strategy, it requires additional complex calculations. Thus, a modulation method for the RSHMC converter is proposed to eliminate the CZCD.

C. Method to Eliminate Current Zero-Crossing Distortion

To eliminate CZCD, a modulation method is proposed in this article, as shown in Figs. 5 and 6.

Taking phase A as an example, when the modulation wave crosses from positive to negative half cycle, the interval where the amplitude of U_a is between 0 and E is defined $A(0, E)$, as shown in Fig. 5. According to the polarity of I_a, $A(0, E)$ is further divided into two subintervals: $A(0, \mathrm{E}, P)$ corresponds to the polarity of I_a is positive and $\mathrm{A}(0, E, N)$ corresponds to the polarity of I_a is negative. When ωt belongs to the subinterval $A(0, E)$, the RSHMC converter should output either 0 level or E level according to the comparison between the triangular carrier and the modulated wave. In the subinterval $A(0, E, P)$, the switching state st6 and st7 can both be selected to output E level and the switching state st5 is selected to output 0 level. However, in the subinterval $A(0, E, N)$, only the switching state st6 which is independent of the polarity of current can be selected to output E level. If the switching state st7 is still selected to output E level in the subinterval $\mathrm{A}(0, E, N)$, the negative current will flow through the diode D_{a1} and the RSHMC converter will output $-3E$ level resulting in the CZCD.

When the modulation wave across from negative to positive half cycle, the interval where the amplitude of U_a is between $-E$ and 0 is defined $A(-E, 0)$, as shown in Fig. 6. According to the polarity of I_a, $A(-E, 0)$ is further divided into two subintervals: $A(-E, 0, N)$ corresponds to the polarity of I_a is negative and $A(-E, 0, P)$ corresponds to the polarity of I_a is positive. When ωt belongs to the subinterval $A(-E, 0)$, the RSHMC converter should output either $-E$ level or 0 level according to the comparison between the triangular carrier and the modulated wave. In the subinterval $A(-E, 0, N)$, the switching state st3 and st4 can both be selected to output $-E$ level and the switching state st5 is selected to output 0 level. However, in the subinterval $A(-E, 0, P)$, only the switching state st4 which is independent of the polarity of current can be selected to output $-E$ level. If the switching state st3 is still selected to output $-E$ level in the subinterval $A(-E, 0, P)$, the positive current will flow through the diode D_{a2} and the RSHMC converter will output $+3E$ level resulting in the CZCD.

The switching states considering the elimination of CZCD are given in Table IV. Besides, PD-SPWM in one fundamental period without zero-crossing current distortion is shown in Fig. 7. Different colors correspond to different switching states, respectively, as shown in Fig. 7.

TABLE IV
SWITCHING STATES WITHOUT CURRENT ZERO-CROSSING DISTORTION

ωt	Voltage level	Switching state	Voltage level	Switching state
A(0, E, N)	0	st5	E	st6
A(0, E, P)	0	st5	E	st6 st7
A(E, 2E)	E	st6 st7	2E	st8
A(2E, 3E)	2E	st8	3E	st9
A(3E, 2E)	3E	st9	2E	st8
A(2E, E)	2E	st8	E	st6 st7
A(E, 0)	E	st6 st7	0	st5
A(0, -E, P)	0	st5	-E	st4
A(0, -E, N)	0	st5	-E	st3 st4
A(-E, -2E)	-E	st3 st4	-2E	st2
A(-2E, -3E)	-2E	st2	-3E	st1
A(-3E, -2E)	-3E	st1	-2E	st2
A(-2E, -E)	-2E	st2	-E	st3 st4
A(-E, 0, N)	-E	st3 st4	0	st5
A(-E, 0, P)	-E	st4	0	st5

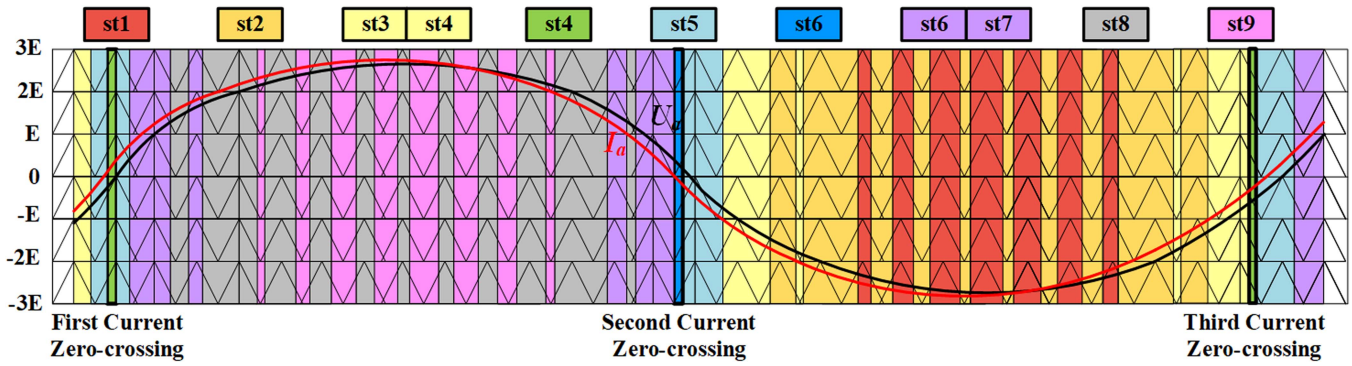

Fig. 7. PD-SPWM without zero-crossing current distortion.

IV. Voltage Balance Modulation Method

Floating capacitor voltage balance and the neutral point voltage are the essential requirements for the stable operation of the RSHMC converter. However, the floating capacitor voltage should be controlled preferentially since the floating capacitor voltage is controlled independently by their own phase. Moreover, for the RSHMC converter, there are redundant switching states which can be used to charge or discharge the capacitor. Thus, to achieve capacitor voltage balance, it is required to select switching state reasonably.

A. Voltage Balance Control of Floating Capacitor

As mentioned above, the floating capacitor voltage should be controlled at E ($U_{\rm dc}/4$). Besides, it can be seen from Fig. 2 and Table II that the switching states st2, st5, and st8 have no effect on the floating capacitor voltage since there is no current flowing through the floating capacitor. While the remaining switching states will have influence on the floating capacitor voltage. For example, when the output voltage is $\pm 3E$, the floating capacitor voltage is uncontrollable since there are no redundant switching states. When the output voltage is $\pm E$, there are two switching states which have opposite influence on the floating capacitor voltage. Thus, it can achieve floating capacitor voltage balance through selecting switching states when the output voltage is -*E* or +E.

Take phase A as an example, the deviation of the floating capacitor voltage of phase A is expressed as

$$\Delta U_{fa} = U_{fa} - U_{\rm dc}/4. \tag{17}$$

The control signal of floating capacitor voltage U_{fa} can be expressed as

$$\text{sig}U_{fa} = I_a \Delta U_{fa} \tag{18}$$

In the subinterval *A*(0, *E, P*), the current is positive. Assuming that $\Delta U_{fa} > 0$, $\text{sig}U_{fa} > 0$, the switching state st7 can be selected to discharge the floating capacitor. If $\Delta U_{fa} < 0$, $\text{sig}U_{fa} < 0$, the switching state st6 can be selected to charge the floating capacitor. In the subinterval *A*(0, -*E, N*), the current is negative. Assuming that $\Delta U_{fa} > 0$, $\text{sig}U_{fa} < 0$, the switching state st3 can be selected to discharge the floating capacitor. If $\Delta U_{fa} < 0$, $\text{sig}U_{fa} > 0$, the switching state st4 can be selected to charge the floating capacitor. Specifically, in the subinterval *A*(0, *E, N*), the current is negative. Only the switching state st6 can be selected to discharge the floating capacitor and it cannot realize charging by selecting the switching states in the subinterval *A*(0, *E, N*). Besides, in the subinterval *A*(0, -*E, P*), the current is positive. Only the switching state st4 can be selected to discharge the floating capacitor and it cannot realize charging by selecting the switching states in the subinterval *A*(0, -*E, P*).

B. Voltage Balance Control of Neutral Point

The deviation of the neutral point voltage is expressed as

$$\Delta U_{\rm dc} = U_N - U_P. \tag{19}$$

The control signal of neutral point voltage $U_{\rm dc}$ can be expressed as

$$\text{sig}U_{\rm dc} = I_a \Delta U_{\rm dc} U_a. \tag{20}$$

As mentioned above, it needs to set a threshold which is defined as ΔX to control the overall capacitor voltage balance. Take phase A as an example, when $|\Delta U_{fa}| > \Delta X$, $\text{sig}U_{fa}$ will be used to control the floating capacitor voltage. When $|\Delta U_{fa}| \leq \Delta X$, $\text{sig}U_{\rm dc}$ will be used to control the neutral point voltage. For example, when the output voltage is $\pm 3E$, $\pm 2E$, and 0, the neutral point voltage is uncontrollable since there are no redundant switching states. When the output voltage is $\pm E$, there are two switching states which have opposite influence on the neutral point voltage. Thus, it can achieve neutral point voltage balance through selecting switching states when the output voltage is -*E* or +*E*.

In the subinterval *A*(0, *E, P*), the current is positive. Assuming that $\Delta U_{\rm dc} > 0$, $\text{sig}U_{\rm dc} > 0$, the switching state st7 can be selected to discharge the capacitor C_{d2}. If $\Delta U_{\rm dc} < 0$, $\text{sig}U_{\rm dc} < 0$, the switching state st6 can be selected to charge the capacitor C_{d2}. In the subinterval *A*(0, -*E, N*), the current is negative. Assuming that $\Delta U_{\rm dc} > 0$, $\text{sig}U_{\rm dc} > 0$, the switching state st4 can be selected to discharge the capacitor C_{d2}. If $\Delta U_{dc} < 0$, $\text{sig}U_{dc} < 0$, the switching state st3 can be selected to charge the capacitor C_{d2}. Specifically, in the subinterval *A*(0, *E, N*), the current is negative. Only the switching state st6 can be selected to discharge the capacitor C_{d2} and it cannot realize charging by selecting the switching states in the subinterval *A*(0, *E, N*). Besides, in the

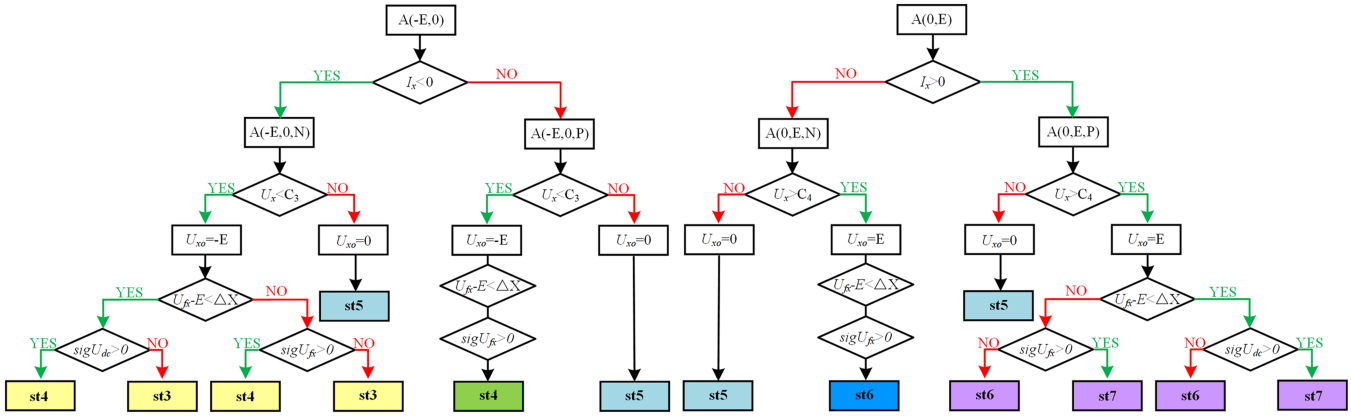

Fig. 8. Flow chart of charge and discharge of capacitors.

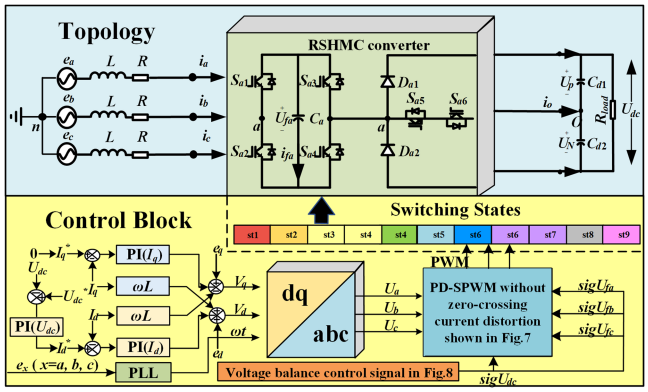

Fig. 9. Control diagram of the RSHMC converter.

TABLE V
SWITCHING STATES OF VOLTAGE BALANCE STRATEGY WHEN $|\Delta U_{FX}| > \Delta X$

ωt	I_x	$sigU_{fx}$	Switching state	C_x
A(0, E, N)	<0	random	st6	discharge
A(0, E, P)	>0	<0	st6	charge
A(0, E, P)	>0	>0	st7	discharge
A(0, -E, P)	>0	random	st4	discharge
A(0, -E, N)	<0	<0	st3	discharge
A(0, -E, N)	<0	>0	st4	charge

TABLE VI
SWITCHING STATES OF VOLTAGE BALANCE STRATEGY WHEN $|\Delta U_{FX}| \leq \Delta X$

ωt	I_x	$sigU_{dc}$	Switching state	C_{d2}
A(0, E, N)	<0	random	st6	discharge
A(0, E, P)	>0	>0	st6	charge
A(0, E, P)	>0	<0	st7	discharge
A(0, -E, P)	>0	random	st4	charge
A(0, -E, N)	<0	<0	st3	charge
A(0, -E, N)	<0	>0	st4	discharge

subinterval $A(0, -E, P)$, the current is positive. Only the switching state st4 can be selected to charge the capacitor C_{d2} and it cannot realize discharging by selecting the switching states in the subinterval $A(0, -E, P)$.

For example, ΔX is set to 5. Take phase A as an example, when $|\Delta U_{fa}| \leq 5$, $\mathrm{sig}U_{\mathrm{dc}}$ will be used to control the neutral point voltage. When $\Delta U_{\mathrm{dc}} > 0$, the switching state st7 can be selected to discharge the capacitor C_{d2} when the output voltage of the RSHMC converter is $+E$ and the switching state st4 can be selected to discharge the capacitor C_{d2} when the output voltage of the RSHMC converter is -E. When $\Delta U_{\mathrm{dc}} < 0$, the switching state st6 can be selected to charge the capacitor C_{d2} when the output voltage of the RSHMC converter is +E and the switching state st3 can be selected to charge the capacitor C_{d2} when the output voltage of the RSHMC converter is -E.

When $|\Delta U_{fa}| > 5$, $\mathrm{sig}U_{fa}$ will be used to control the floating capacitor voltage balance. When the RSHMC converter operates in the steady state, the floating capacitor voltage will fluctuate within the set value of +5 V or -5 V. If ΔU_{fa} is greater than +5 V, the switching state st7 can be selected to discharge the floating capacitor when the output voltage of the RSHMC converter is +E and the switching state st3 can be selected to discharge the floating capacitor when the output voltage of the RSHMC converter is -E. If ΔU_{fa} is less than -5 V, the switching state st6 can be selected to charge the floating capacitor when the output voltage of the RSHMC converter is $+E$ and the switching state st4 can be selected to charge the floating capacitor when the output voltage of the RSHMC converter is -E.

The switching states of the voltage balance strategy for the RSHMC converter are given in Tables V and VI. Besides, flow chart of charge and discharge of the capacitors is shown in Fig. 8.

In summary, Fig. 9 depicts the control diagram of the RSHMC converter. The phase-locked loop shown in Fig. 9 captures the grid voltage phase to facilitate the dq transformation. In the dq

TABLE VII
SIMULATION AND EXPERIMENTAL PARAMETERS

Parameters	Simulation	Experiment
DC-link voltage (U_{dc})	540 V/590 V/680 V	95 V/105 V/120 V
Grid voltage (V_g)	311 V	55 V
Filter resistance (R)	0.5 Ω	0.5 Ω
Filter inductor (L)	5 mH	5 mH
Resistance load (R_{load})	12 Ω	12 Ω/9 Ω
DC-side capacitor (C_{d1}, C_{d2})	2350 μF	2350 μF
Floating capacitor (C_{fx})	3333 μF	3333 μF
Control period (T_s)	100 μs	100 μs
Line frequency (f_{line})	50 Hz	50 Hz

domain, I_d* and I_q* serve as the current references, while I_d and I_q correspond to the three-phase currents after the dq conversion, as illustrated in Fig. 9.

V. SIMULATION AND EXPERIMENTAL RESULTS

To verify the effectiveness of the modulation method illustrated above, the model of the RSHMC converter is established in MATLAB/SIMULINK. Table VII gives the simulation and experimental parameters. When the dc-link voltage $U_{\rm dc}$ is 540V/590V/680V and the grid voltage V_g is 311 V, the modulation index m is 1/0.9/0.8 in simulation. When the dc-link voltage $U_{\rm dc}$ is 95V/105V/120V and the grid voltage V_g is 55 V, the modulation index m is 1/0.9/0.8 in experiment. In this section, the modulation method with CZCD elimination and voltage balance control for the RSHMC converter is verified its feasibility and effectiveness.

A. Simulation Results

The simulation results when modulation index m is 0.8 are shown in Fig. 10. As shown in Fig. 10(a) and (b), the output phase voltage is five-level and the line voltage is nine-level. In Fig. 10(c)–(e), the output three-phase current, the voltage of the three-phase floating capacitor and the dc-link capacitor voltage are all controllable and balanced. It is obvious that there is no CZCD in the output current of the RSHMC converter with the proposed modulation method.

Fig. 11 shows the simulation results when modulation index m is 1. As shown in Fig. 11(a) and (b), the output phase voltage is seven-level and the line voltage is eleven-level. There is no CZCD and the output current is balanced and low harmonic, as shown in Fig. 11(c). Besides, the three-phase floating capacitors and the dc-link capacitor voltage are both controllable with the proposed modulation method when modulation index m is 1.

To verify the effectiveness of the proposed modulation method, Fig. 12 shows transient simulation results when modulation index m is 0.9. From 0.4 to 0.5 s, the RSHMC converter adopts the modulation method without eliminating the CZCD to control the voltage balance of the floating capacitors and the dc-link.

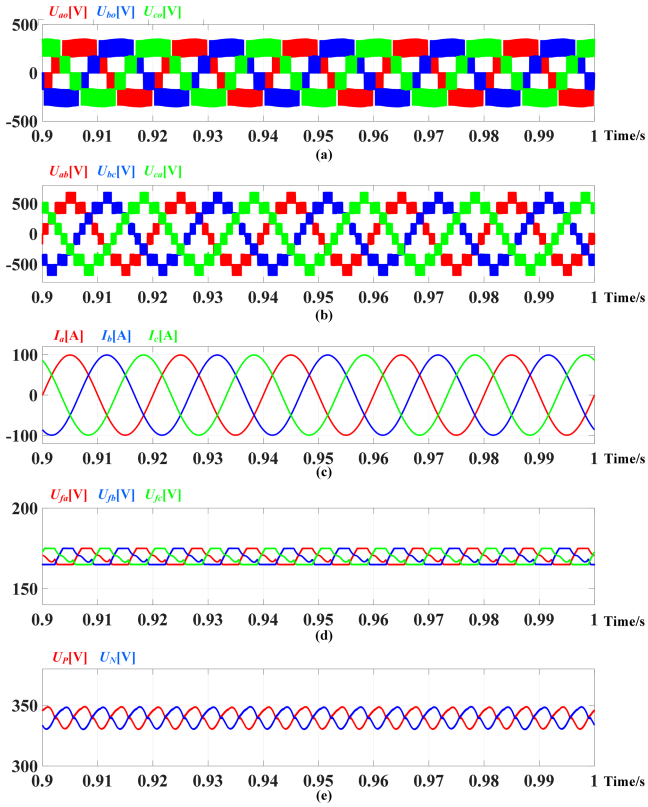

Fig. 10. Simulation results when modulation index $m = 0.8$, including (a) phase voltage, (b) line voltage, (c) three-phase current, (d) voltages of the floating capacitors, and (e) the upper and lower capacitor voltages of DC-link.

As shown in Fig. 12(c), there is distortion when the current crossing the zero point. Besides, the voltage of three-phase floating capacitors and the dc-link capacitor is not well balanced before 0.5 s, as shown in Fig. 12(d) and (e). At 0.5 s, the RSHMC converter adopts the proposed modulation method to eliminate the CZCD and to control the voltage balance of the floating capacitors and the dc-link. After adopting the proposed modulation method, the output phase voltage returns to balanced seven levels and the line voltage returns to balanced eleven levels, as shown in Fig. 12(a) and (b). It is worth mentioned that the current restores balance without CZCD, as shown in Fig. 12(c). Besides, the voltage of the floating capacitors and the dc-link voltage are balanced with less fluctuation, as shown in Fig. 12(d) and (e).

B. Experimental Results

The experiment is conducted in the RSHMC converter platform to verify the feasibility of the proposed modulation method. The experimental prototype of the RSHMC converter is shown in Fig. 13 and the experimental parameters are given in Table VII. In the experiment, the Infineon switch IGBT (part no. IKW40N120T2) is used. In the measurement tools selection, the current sensors (part no.T60404-N4646-X400) and the voltage sensors (part no.VSM025A) are to transmit the signals to the dspace controller and the current probes and the voltage probes are to transmit the signals to the oscilloscope. The Tektronix

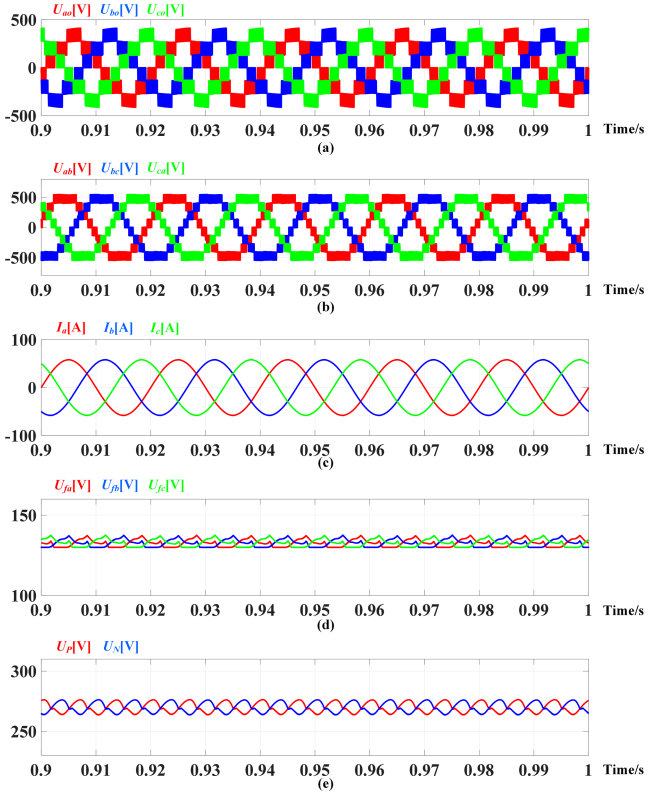

Fig. 11. Simulation results when modulation index m = 1, including (a) phase voltage, (b) line voltage, (c) three-phase current, (d) voltages of the floating capacitors, and (e) the upper and lower capacitor voltages of DC-link.

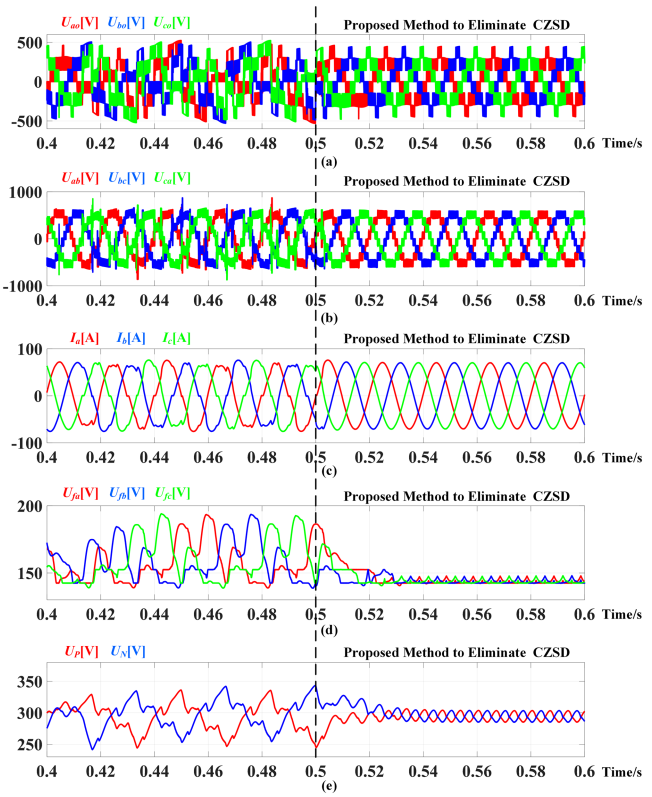

Fig. 12. Transient simulation results when modulation index $m = 0.9$, including (a) phase voltage, (b) line voltage, (c) three-phase current, (d) voltages of the floating capacitors, and (e) the upper and lower capacitor voltages of DC-link.

TPS 2014B oscilloscope is utilized to observe and record the experimental results.

The experimental results when modulation index m is 0.8, 0.9, and 1 are, respectively, shown in Figs. 14 –16. When the dc-side voltage decreases from 120 to 95 V, the corresponding modulation index m will increase from 0.8 to 1 and the phase current will decrease correspondingly. Besides, with the increase of the modulation index m, the output phase voltage level increases from five-level in Fig. 14(a) to seven-level in Figs. 15(a) and 16(a). Furthermore, Figs. 14–16 jointly show that the output phase currents are all undistorted and balanced and the voltage of the floating capacitor and the voltage of dc-side are all balanced and well-controlled which can verify the effectiveness of the proposed modulation method.

Fig. 17 shows the transient experimental results when modulation index $m = 0.9$ from $R = 12\ \Omega$ to $R = 9\ \Omega$. When the resistance load decreases, the current of phase A will increase, as shown in Fig. 17. Besides, after switching the resistance load, the floating capacitor voltage and the voltage of dc-side are still balanced and well-controlled.

Fig. 18 shows the transient experimental results when modulation index $m = 0.9$ from adopting voltage balance method without eliminating CZCD to adopting the proposed modulation method. When adopting voltage balance method without eliminating CZCD, the phase current is distorted and the floating

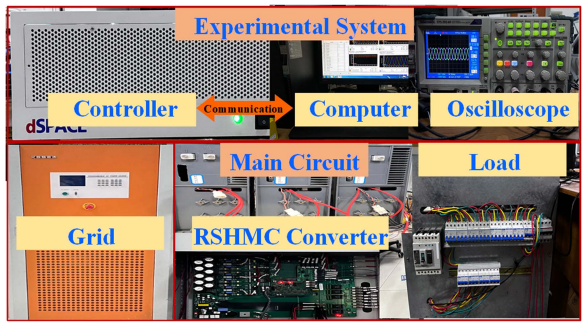

Fig. 13. Experimental prototype of the RSHMC converter.

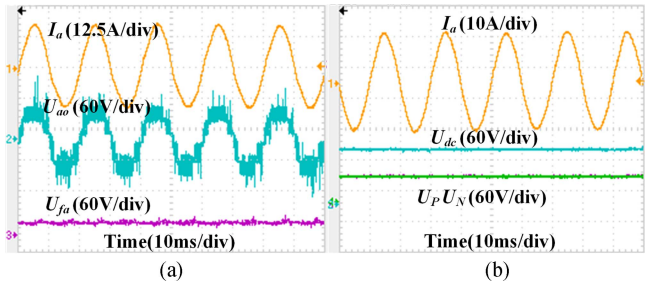

Fig. 14. Experimental results when modulation index $m = 0.8$, including (a) output current of phase A (I_a), output voltage of phase A (U_{ao}) and the floating capacitor voltage of phase A (U_{fa}) and (b) voltage of DC-side ($U_{\rm dc}$) and the upper and lower capacitor voltages of DC-side (U_P, U_N).

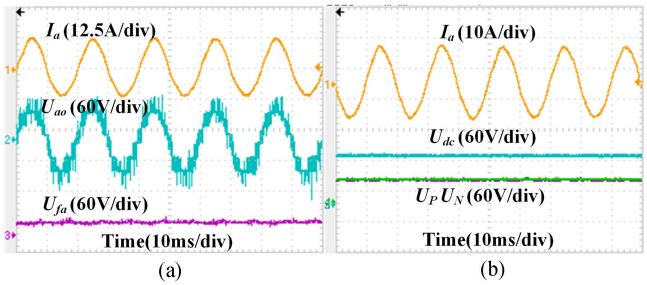

Fig. 15. Experimental results when modulation index $m = 0.9$, including (a) output current of phase A (I_a), output voltage of phase A (U_{ao}) and the floating capacitor voltage of phase A and (b) voltage of dc-side ($U_{\rm dc}$) and the upper and lower capacitor voltages of dc-side (U_P, U_N).

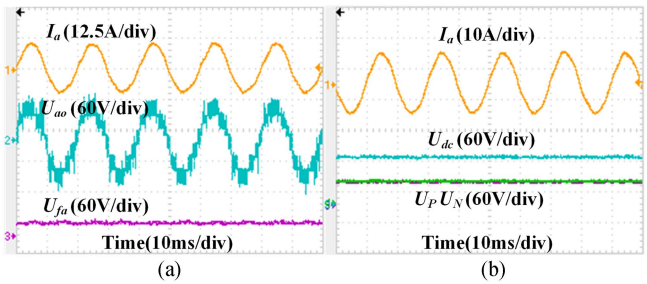

Fig. 16. Experimental results when modulation index $m = 1$, including (a) output current of phase A (I_a), output voltage of phase A (U_{ao}) and the floating capacitor voltage of phase A and (b) voltage of DC-side ($U_{\rm dc}$) and the upper and lower capacitor voltages of DC-side (U_P, U_N).

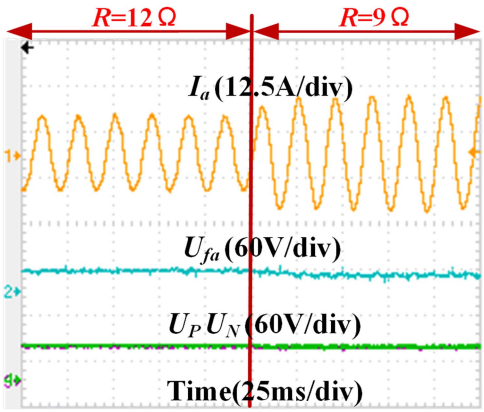

Fig. 17. Transient experimental results when modulation index $m = 0.9$ from $R = 12\ \Omega$ to $R = 9\ \Omega$, including output current of phase A (I_a), the floating capacitor voltage of phase A and the upper and lower capacitor voltages of dc-side (U_P, U_N).

capacitor voltage and the voltage of the dc-side deviate from the set voltage. After adopting the proposed modulation method, there is no distortion in the phase current and the floating capacitor voltage and the voltage of dc-side restore balance. Therefore, the proposed modulation method is effective and well performed.

Fig. 19 shows the FFT analysis in experiment of the current and its spectrum after adopting the voltage balance method without eliminating CZCD under $m = 0.9$ and adopting the

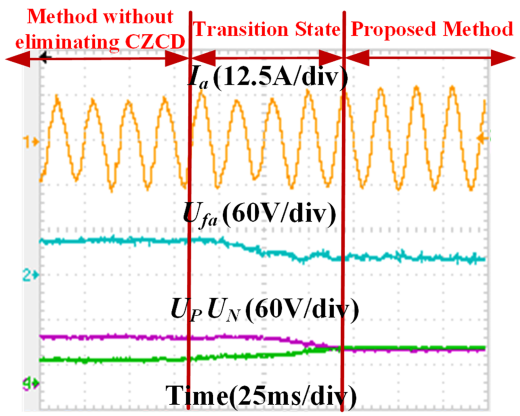

Fig. 18. Transient experimental results when modulation index $m = 0.9$ from adopting voltage balance method without eliminating CZCD to adopting the proposed modulation method, including output current of phase A (I_a), the floating capacitor voltage of phase A and the upper and lower capacitor voltages of dc-side (U_P, U_N).

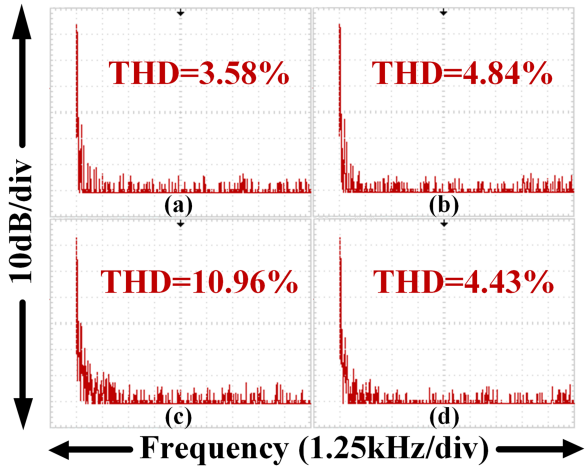

Fig. 19. FFT analysis in experiment of the current and its spectrum. (a) Adopting the proposed modulation method under $m = 0.8$. (b) Adopting the proposed modulation method under $m = 1$. (c) Adopting the voltage balance method without eliminating CZCD under $m = 0.9$. (d) Adopting the proposed modulation method under $m = 0.9$.

proposed modulation method under $m = 0.8$, 0.9 and 1. The THD of the current are respectively 3.58% and 4.84% when the modulation index m is 0.8 and 1, as shown in Fig. 19(a) and (b). When the modulation index m is 0.9, the THD of the current decreases from 10.96% to 4.43% after adopting the proposed modulation method to eliminate CZCD.

VI. Conclusion

In this article, a modulation method with CZCD elimination and voltage balance control for the RSHMC converter was proposed. The proposed modulation method can eliminate the CZCD of the RSHMC converter by reasonably selecting redundant switching states. Besides, the floating capacitor voltage and the neutral point voltage can be balanced by utilizing different charge or discharge switching states. Since both the voltage control of the floating capacitor and the neutral point need to

utilize the switching states, a threshold was set to control the overall capacitor voltage balance. After adopting the proposed modulation method, the current quality was improved compared with adopting the method without eliminating CZCD and the THD of current was controlled to less than 5% with no CZCD and balanced voltage. Besides, the proposed modulation method is also effective under multiple modulation index and under dynamic conditions which can ensure the normal operation of the RSHMC converter under different working conditions. The simulation and experimental results have confirmed the feasibility and validity of the proposed modulation method.

REFERENCES

[1] M. Zhang, Z. Zhang, Z. Li, H. Chen, and D. Zhou, "A unified open-circuit-fault diagnosis method for three-level neutral-point-clamped power converters," *IEEE Trans. Power Electron.*, vol. 38, no. 3, pp. 3834–3846, Mar. 2023.

[2] H. Yuan, H. S. Lam, N. Beniwal, S. -C. Tan, J. Pou, and S. -Y. R. Hui, "Direct-switch duty-cycle control of grid-connected n-level neutral-point-clamped converter," *IEEE Trans. Ind. Electron.*, vol. 70, no. 9, pp. 8624–8633, Sep. 2023.

[3] A. Lewicki, C. Odeh, and M. Morawiec, "Space vector pulsewidth modulation strategy for multilevel cascaded H-bridge inverter with DC-link voltage balancing ability," *IEEE Trans. Ind. Electron.*, vol. 70, no. 2, pp. 1161–1170, Feb. 2023.

[4] R. Zhang, C. Zhang, X. Xing, X. Liu, and F. Blaabjerg, "Clustered voltage control and modulation scheme with switching loss reduction for high power hybrid cascaded converter," *IEEE Trans. Ind. Electron.*, vol. 71, no. 5, pp. 4911–4921, May 2024, doi: 10.1109/TIE.2023.3283687.

[5] Q. Xiao et al., "An improved fault-tolerant control scheme for cascaded H-bridge STATCOM with higher attainable balanced line-to-line voltages," *IEEE Trans. Ind. Electron.*, vol. 68, no. 4, pp. 2784–2797, Apr. 2021.

[6] Q. Xiao et al., "Modulated model predictive control for multilevel cascaded H-bridge converter-based static synchronous compensator," *IEEE Trans. Ind. Electron.*, vol. 69, no. 2, pp. 1091–1102, Feb. 2022.

[7] C. Wen, X. Xing, C. Liu, L. Xing, R. Zhang, and B. Liu, "An improved model predictive control for a novel flying-capacitor five-level converter with reduced switching devices," *IEEE J. Emerg. Sel. Topics Power Electron.*, vol. 11, no. 5, pp. 4969–4981, Oct. 2023.

[8] A. Ghias, J. Pou, V. Agelidis, and M. Ciobotaru, "Initial capacitor charging in grid-connected flying capacitor multilevel converters," *IEEE Trans. Power Electron.*, vol. 29, no. 7, pp. 3245–3249, Jul. 2014.

[9] X. Xing, Z. Zhang, C. Zhang, J. He, and A. Chen, "Space vector modulation for circulating current suppression using deadbeat control strategy in parallel three-level neutral-clamped converters," *IEEE Trans. Ind. Electron.*, vol. 64, no. 2, pp. 977–987, Feb. 2017.

[10] Q. Xiao et al., "Review of fault diagnosis and fault-tolerant control methods of the modular multilevel converter under submodule failure," *IEEE Trans. Power Electron.*, vol. 38, no. 10, pp. 12059–12077, Oct. 2023.

[11] S. Mariethoz, "Systematic design of high-performance hybrid cascaded multilevel converters with active voltage balance and minimum switching losses," *IEEE Trans. Power Electron.*, vol. 28, no. 7, pp. 3100–3113, Jul. 2013.

[12] B. Zhang, C. Zhang, X. Xing, X. Li, and Z. Chen, "Novel three-layer discontinuous PWM method for mitigating resonant current and zero-crossing distortion in Vienna rectifier with an LCL filter," *IEEE Trans. Power Electron.*, vol. 36, no. 12, pp. 14478–14490, Dec. 2021.

[13] H. Yu, B. Chen, W. Yao, and Z. Lu, "Hybrid seven-level converter based on T-type converter and H-Bridge Cascaded under SPWM and SVM," *IEEE Trans. Power Electron.*, vol. 33, no. 1, pp. 689–702, Jan. 2018.

[14] H. Liu, C. Liu, X. Xing, and C. Zhang, "A reduced switch hybrid multilevel converter with coordinated control method for current distortion mitigation and capacitor voltages balancing," *IEEE J. Emerg. Sel. Topics Power Electron.*, vol. 12, no. 1, pp. 593–606, Feb. 2024.

[15] Y. Chen and J. He, "Fault detection and ride through of CHB converter-based star-connected STATCOM through exploring the inherent information of multiloop controllers," *IEEE Trans. Power Electron.*, vol. 38, no. 2, pp. 1366–1371, Feb. 2023.

[16] Z. Cheng and B. Wu, "A novel switching sequence design for five-level NPC/H-bridge inverters with improved output voltage spectrum and minimized device switching frequency," *IEEE Trans. Power Electron.*, vol. 22, no. 6, pp. 2138–2145, Nov. 2007.

[17] J. Meili, S. Ponnaluri, L. Serpa, P. K. Steimer, and J. W. Kolar, "Optimized pulse patterns for the 5-level ANPC converter for high speed high power applications," in *Proc. IEEE 32nd Annu. Conf. Ind. Electron.*, 2006, pp. 2587–2592.

[18] M. Narimani, B. Wu, Z. Cheng, and N. R. Zargari, "A new nested neutral point-clamped (NNPC) converter for medium-voltage (MV) power conversion," *IEEE Trans. Power Electron.*, vol. 29, no. 12, pp. 6375–6382, Dec. 2014.

[19] W. Zhu, X. Li, X. Cao, Y. Li, and K. Zhou, "An improved modulation strategy without current zero-crossing distortion and control method for vienna rectifier," *IEEE Trans. Power Electron.*, vol. 38, no. 12, pp. 15199–15213, Dec. 2023.

[20] D. Molligoda et al., "Hybrid modulation strategy for the vienna rectifier," *IEEE Trans. Power Electron.*, vol. 37, no. 2, pp. 1283–1295, Feb. 2022.

[21] J. Chen, C. Zhang, A. Chen, X. Xing, and F. Gao, "A carrier-based fault-tolerant control strategy for T-type rectifier with neutral-point voltage oscillations suppression," *IEEE Trans. Power Electron.*, vol. 34, no. 11, pp. 10988–11001, Nov. 2019.

[22] J. W. Kolar and F. C. Zach, "A novel three-phase utility interface minimizing line current harmonics of high-power telecommunications rectifier modules," *IEEE Trans. Ind. Electron.*, vol. 44, no. 4, pp. 456–466, Aug. 1997.

[23] A. Rajaei, M. Mohamadian, and A. Y. Varjani, "Vienna-rectifier-based direct torque control of PMSG for wind energy application," *IEEE Trans. Ind. Electron.*, vol. 60, no. 7, pp. 2919–2929, Jul. 2013.

[24] H. Chen and D. C. Aliprantis, "Analysis of squirrel-cage induction generator with VIENNA rectifier for wind energy conversion system," *IEEE Trans. Energy Convers.*, vol. 26, no. 3, pp. 967–975, Sep. 2011.

[25] Fusheng Wang, Yunliang Teng, Zhaoshuan Yuan, and Jiayi Xu, "A maximum power factor of control algorithms of three-level Vienna rectifier without current distortion at current zero-crossing point," in *Proc. IEEE 8th Int. Power Electron.*, 2016, pp. 2325–2331.

[26] J. Wang, S. Ji, S. Liu, H. Jiang, and W. Jiang, "A discontinuous PWM strategy to control neutral point voltage for Vienna rectifier with improved PWM sequence," *IEEE J. Emerg. Sel. Topics Power Electron.*, vol. 10, no. 3, pp. 3230–3241, Jun. 2022.

[27] L. Song, S. Duan, R. Li, X. Liu, and B. Ji, "A hybrid discontinuous PWM strategy for current ripple and neutral-point fluctuation reduction of parallel Vienna rectifier," *IEEE Trans. Ind. Electron.*, vol. 70, no. 3, pp. 2531–2542, Mar. 2023.

[28] L. Zhang et al., "A modified DPWM with neutral point voltage balance capability for three-phase Vienna rectifiers," *IEEE Trans. Power Electron.*, vol. 36, no. 1, pp. 263–273, Jan. 2021.

[29] L. Dalessandro, S. D. Round, U. Drofenik, and J. W. Kolar, "Discontinuous space-vector modulation for three-level PWM rectifiers," *IEEE Trans. Power Electron.*, vol. 23, no. 2, pp. 530–542, Mar. 2008.

[30] L. Hang, M. Zhang, B. Li, L. Huang, and S. Liu, "Space vector modulation strategy for VIENNA rectifier and load unbalanced ability," *IET Power Electron*, vol. 6, no. 7, pp. 1399–1405, Aug. 2013.

[31] H. Liu, C. Zhang, X. Li, X. Xing, and C. Liu, "Improved model predictive control strategy for hybrid seven-level converter," in *Proc. IEEE Int. Conf. Predictive Control Electr. Drives Power Electron.*, 2021, pp. 51–56.

[32] J.-S. Lee and K.-B. Lee, "A novel carrier-based PWM method for Vienna rectifier with a variable power factor," *IEEE Trans. Ind. Electron.*, vol. 63, no. 1, pp. 3–12, Jan. 2016.

Guangtao Zhou (Student Member, IEEE) was born in Daqing, China, in 2000. He received the B.S. degree in automation from Shandong University, Jinan, China, in 2022. He is currently working toward the M.S. degree in electrical engineering with the School of Control Science and Engineering, Shandong University, Jinan, China.

His current research interests include fault-tolerance and hybrid multi-level converters.

Xiangyang Xing (Member, IEEE) was born in Rizhao, Shandong Province, China, in 1985. He received the B.S. degree in automation and the M.S. degree in control theory and application degree from Qufu Normal University, Jining, China, in 2009 and 2012, and the Ph.D. degree in electrical engineering from Shandong University, Jinan, China, in 2016.

From 2017 to 2019, he was a Post-Doctoral Research Fellow with Shandong University, Jinan, China. In 2019, he was with Shandong University, where he is currently a Full Professor with the School of Control Science and Engineering. His current research interests include multi-level converters, power conversion, and renewable power generation.

Hao Liu (Student Member, IEEE) was born in Shandong, China, in 1998. He received the B.S. degree in electrical engineering and automation from Northeast Electrical Power University Jilin, China, in 2020. He is currently working toward the M.S. degree in electrical engineering with the School of Control Science Engineering, Shandong University, Jinan, China.

His current research interests include topologies and control strategies of multilevel converters.

Shuai Zhang (Member, IEEE) was born in Dezhou, Shandong Province, China, in 1991. He received the B.S. degree in electrical engineering from Qingdao University, China, in 2013, and the Ph.D. degree in electrical engineering from Tianjin University, Tianjin, China, in 2019.

From 2019 to 2022, he was a Post-Doctoral Research Fellow with Shandong University, Jinan, China. In 2022, he was with Shandong University, where he is currently an Associate Researcher with the School of Control Science and Engineering.

His current research interests include renewable power generation and new energy power system stability control.

Xiangjun Li (Senior Member, IEEE) received the Ph.D. degree in electrical and electronic engineering from the Kitami Institute of Technology, Kitami, Japan, in March 2006.

He has been the Director with Energy Storage System Integration and Configuration Technology Research Laboratory, Energy Storage and Electrotechnics Department, China Electric Power Research Institute, since June 2019. Prior to join the China Electric Power Research Institute, Beijing, China, in March 2010, he was a Post-Doctoral Research Fellow and an Assistant Research Professor with Tsinghua University, Beijing, China, from 2008 to 2010. He was a Post-Doctoral Research Fellow with the Korea Institute of Energy Research, Daejeon, South Korea, from 2006 to 2007, respectively. He has authored or coauthored more than 150 technical papers, more than 120 patents, and six books. His current research interests include the topic of digital intelligence/planning configuration/integration/SCADA/operation control/application technologies for energy storage system/stations, distributed generation systems, electric vehicle, and microgrids.

Dr. Li is a Fellow of IET, a Chartered Engineer of U.K., and is one of the Senior Members of CSEE, CAS, and CES. He was a recipient of the Advanced Individual in Science and Technology Work Award of State Grid Corporation of China, the CSEE China Electric Power Excellent Scientific and Technological Worker Award, First Batch Excellent Individuals in the Energy Storage Field of China-EU Energy Technology Innovation Cooperation, National Energy Administration of China, and IEEE PES China Satellite Technology Committee Distinguished Individual Contribution Award.

Rui Zhang (Student Member, IEEE) was born in Shandong, China, in 1997. He received the B.S. degree in electrical engineering from Hefei University of Technology, Hefei, China, in 2019. He is currently working toward the Ph.D. degree in electrical engineering with the School of Control Science and Engineering, Shandong University, Jinan, China.

His current research interests include control strategy of multilevel converters and power quality management.